scientific reports

Check for updates

OPEN

Membrane tubulation induced by a bacterial glycolipid

Kaoru Nomura[1]✉, Akihiro Tsuji[2], Hayato Yamashita[2], Masayuki Abe[2], Kohki Fujikawa[1], Shoko Mori[1], Tsukiho Osawa[1], Hiromi Toyonaga[1], Tomohiro Osugi[1], Kazuma Yasuhara[3], Kenichi Morigaki[4], Ken-ichi Nishiyama[5] & Keiko Shimamoto[1,6]✉

Membrane protein integrase (MPIase) is a glycolipid found in *Escherichia coli* cell membranes. It consists of diacylglycerol and a sugar chain comprising approximately 10 repeating trisaccharide units, made up of three types of *N*-acetylated amino sugars linked by pyrophosphate. In cooperation with proteinaceous translocons, MPIase regulates membrane protein integration. In this study, using various microscopic techniques, we demonstrated that externally added MPIase induces the formation of a single tubule protruding outward from giant unilamellar vesicles (GUVs). These tubules resembled those reported in studies involving membrane-perturbing proteins but differed in that MPIase formed aggregates at the base of the tubules. We also showed that hydrophobic interactions between longer sugar chains of MPIase play a key role in forming multiple aggregates on the membrane, which in turn induce membrane budding and triggers membrane protrusion. Once a single tubule begins to form from one of the aggregates, elongating a longer and narrower tubule can reduce line tension and elastic energy for a given area differences between the internal and external leaflets. These findings provide insights into the mechanism underlying glycolipid-induced membrane tubulation and suggest that the unique long sugar chain of MPIase can offer functions beyond its essential role in membrane protein integration.

Membrane protein integrase (MPIase) is an essential glycolipid in *Escherichia coli* (*E. coli*) that plays a crucial role in membrane protein integration[1–3]. It is located in the inner membrane of *E. coli*, facilitating the integration of nascent proteins synthesized by ribosomes on the cytoplasmic side of the membrane. Membrane proteins with multiple transmembrane domains use Sec translocons for integration in a Sec-dependent process[4–6], whereas smaller hydrophobic proteins do not require such assistance, i.e., a Sec-independent process[7,8]. MPIase is essential for both processes. MPIase possesses a sugar chain with approximately 10 repeating trisaccharide units linked to diacylglycerol (DAG) via pyrophosphate (Fig. 1a)[3]. The sugar chain comprises three types of acetylated amino sugars: 2-acetamido-2-deoxyglucose (GlcNAc), 2-acetamido-2-deoxymannuronic acid, and 4-acetamido-4-deoxyfucose, with about one-third of the GlcNAc residues *O*-acetylated at the 6-position[3]. We previously showed that the structural features of MPIase are critical for interactions with substrate proteins during Sec-independent membrane protein integration[9–12].

Hydrophobic interactions between the acetyl groups of MPIase and the hydrophobic residues of substrate proteins as well as electrostatic interactions between the carboxylate groups of MPIase and the basic residues of substrate proteins are important for capturing proteins released from the ribosomal tunnel and preventing aggregation. Additionally, MPIase's long, flexible sugar chains allow rapid association and dissociation with substrate proteins, efficiently delivering them to the membrane surface[11]. Electrostatic interactions between MPIase's pyrophosphate and basic residues of membrane proteins are crucial for attracting proteins to the membrane surface[9,12].

Our prior research indicated that MPIase's long, flexible sugar chain loosens membrane surface packing and increases the mobility in the membrane core[12,13]. DAG, a minor lipid component in the *E. coli* membrane, blocks unregulated spontaneous membrane integration[14]. DAG's compact structure, with two fatty acid chains ester-bonded to a glycerol moiety, fits under the polar groups of other membrane lipids, increasing acyl chain

[1]Bioorganic Research Institute, Suntory Foundation for Life Sciences, 8-1-1 Seikadai, Seika- cho, Soraku-gun, Kyoto 619-0284, Japan. [2]Graduate School of Engineering Science, Osaka University, 1-3 Machikaneyama, Toyonaka 560-8531, Osaka, Japan. [3]Division of Materials Science, Nara Institute of Science and Technology (NAIST), 8916-5 Takayama-cho, Ikoma 630-0192, Japan. [4]Biosignal Research Center, Kobe University, 1-1 Rokkodaicho, Nada, Kobe 657-8501, Japan. [5]Department of Biological Chemistry and Food Sciences, Faculty of Agriculture, Iwate University, 3-18-8 Ueda, Morioka 020-8550, Iwate, Japan. [6]Department of Chemistry, Graduate School of Science, Osaka University, 1-1 Machikaneyama, Toyonaka 560-0043, Osaka, Japan. ✉email: nomura@sunbor.or.jp; shimamot@sunbor.or.jp

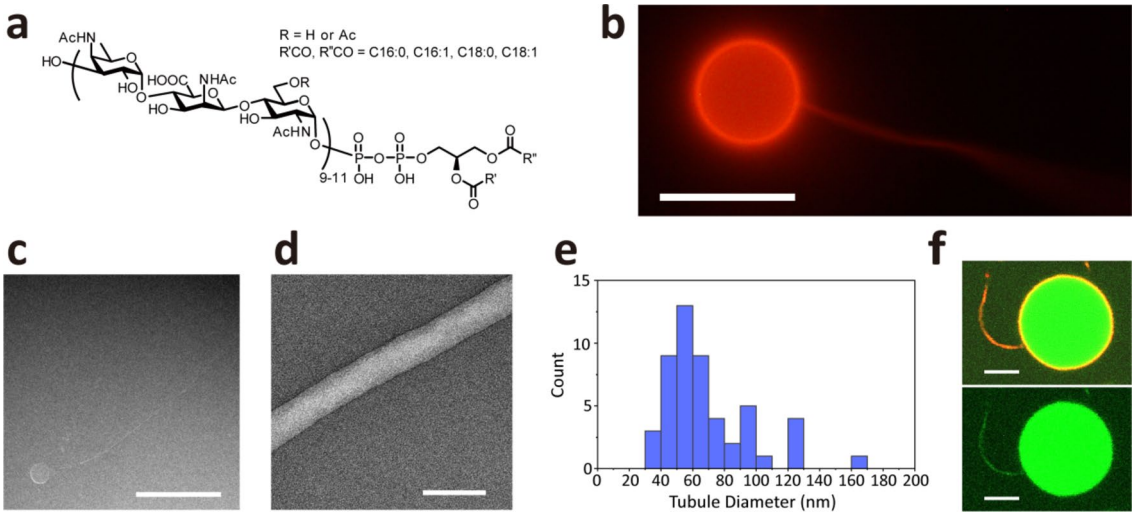

Fig. 1. (**a**) Molecular structure of MPIase. Approximately one-third of the GlcNAc residues are *O*-acetylated at the 6-position. The number of repeating trisaccharide units ranged from 7 to 14, with most between 9 and 11. (**b**) Confocal fluorescence microscopy image of tubule-forming 1-palmitoyl-2-oleoyl-*sn*-glycero-3-phosphocholine (POPC) giant unilamellar vesicles (GUVs) after adding 20 mol% MPIase and incubating for 2 h. The GUVs were visualized by adding 0.1 mol% Texas Red 1,2-dihexadecanoyl-*sn*-glycero-phosphoethanolamine (TR-DHPE). Scale bar: 10 µm. (**c**) Negative-stain electron microscopy (EM) image of a POPC GUV after adding 20 mol% MPIase. Scale bar: 5 µm. (**d**) Higher magnification of the tubule in (**c**). Scale bar: 100 nm. (**e**) Histogram of lipid tubule diameters formed by 20 mol% MPIase, based on the negative-stain EM analysis in (**c**) and (**d**). The average outer diameter of the tubules was 68.0 ± 27.7 nm, with the error representing standard deviation ($n = 51$). (**f**) Confocal image of POPC/0.1% TR-DHPE GUVs encapsulating 1 µM 6-carboxyfluorescein after externally adding 10 mol% MPIase (top). The dye is also visible inside the tubules (bottom). Scale bars: 10 µm.

order and blocking membrane integration. MPIase counteracts this blockage, allowing proteins to access the membrane core.

MPIase's unique structure may also affect membrane curvature and morphology. We thus investigated MPIase's effects on membrane morphology using various microscopic techniques. During these investigations, we observed MPIase inducing the formation of a single elongated membrane tubule from giant unilamellar vesicles (GUVs), often used as a model for cell membranes.

Only a few glycolipids are known to be capable of inducing membrane morphological changes. A well-known example involves the multivalent binding of bacterial toxins, such as cholera toxin, to sphingoglycolipids, resulting in endocytosis of the pathogen protein into the host cell[15]. Glycolipids can also induce membrane shape changes without other molecules, as observed with ganglioside GM1, a member of the sphingoglycolipid family. GM1 induces tubule formation on the bilayer leaflet of GUVs, either inner or outer, that have a higher GM1 distribution[16]. This report on GM1 contains the only description of glycolipid-induced membrane tubulation, and the general mechanisms underlying this tubulation remain unidentified. Lipopolysaccharide (LPS)[17,18], the major glycolipid in the outermost layer of gram-negative bacterial cells, also induces membrane shape changes. Adding LPS to prolate GUVs changes their shape: first they become pear-shaped, before forming two asymmetric spheres connected by a narrow neck[18], although no tubules are formed. LPS shares features with MPIase, such as being a bacterial glycolipid with long sugar chains; however, their mode of membrane deformation differs. Both the factors in glycolipids that cause tubulation and the underlying mechanism remain unclear.

In this study, we investigated MPIase-induced membrane tubulation. We found that MPIase aggregates on membranes through hydrophobic interactions among its long sugar chains, leading to the formation of a single elongated tubule. MPIase maintains aggregates at the tubule base, revealing a novel mechanism for glycolipid-induced membrane tubulation. We compare this membrane deformation mechanism to those involving GM1, LPS, and scaffolding[19–23]or membrane-bound[24,25] proteins. Overall, this study highlights the diverse roles of glycolipids in membrane dynamics and provides insights into glycolipid function in cellular processes.

Results

Membrane tubulation induced by MPIase

To examine MPIase's effect on liposomes, we prepared GUVs from a mixture of 1-palmitoyl-2-oleoyl-*sn*-glycero-3-phosphocholine (POPC) and 0.1% Texas Red 1,2-dihexadecanoyl-*sn*-glycero-phosphoethanolamine (TR-DHPE). After GUV formation, MPIase was added to the GUVs in buffer A [25 mM Tris-HCl and 50 mM KCl, (pH 7.6)] at a molar ratio of 20 mol% to the GUV lipids. We observed a tubule protruding from the GUV (Fig. 1b). As the GUVs formed before MPIase addition, MPIase localized asymmetrically in the outer leaflet of the lipid bilayer. Microscopic observation throughout the entire depth of GUVs revealed that nearly all tubule-forming GUVs had a single elongated tubule after 2 h of incubation. The tubules were formed from GUVs of

various sizes. Thirty minutes after the addition of MPIase, most GUVs had not yet formed tubules. Although a few GUVs had formed tubules, the tubules were already long and no GUVs with short tubules in the process of forming were observed. Note that, adding 20 mol% MPIase to POPC large unilamellar vesicles (LUVs) resulted in only 5.2 mol% being adsorbed onto the membrane (Figure S1). Therefore, the actual mol% of MPIase on the membrane was much less than added outside. Since LUVs have a higher curvature than GUVs, it is likely that even less MPIase is actually inserted into the GUVs than would be inferred from the analysis using the LUVs shown in Figure S1.

Tubule formation in the presence of MPIase was also observed in the negative-stain electron microscopy (EM) image (Fig. 1c). As observed in the confocal microscopy image (Fig. 1b), POPC GUVs had a single and long tubule extending across the entire observed area. At higher magnification (Fig. 1d), the average tubule diameter was 68.0 ± 27.7 nm (n = 51; Fig. 1e). To determine if the tubules were filled with buffer solution, we prepared POPC/0.1 mol% TR-DHPE GUVs in buffer containing 6-carboxyfluorescein dye. After diluting the GUV solution 100-fold in buffer A, the dye remained inside the GUVs. Upon applying 20 mol% MPIase, tubules formed, and the dye was observed in both the tubule and GUVs, indicating that the tubules were hollow rather than rod-shaped (Fig. 1f).

To confirm that MPIase causes tubulation, we evaluated tubule frequency at various concentrations. The proportion of tubule-forming vesicles increased with higher MPIase concentrations on the membrane (Fig. 2a). Below 5 mol%, tubule-forming vesicles increased with MPIase concentration; above 5 mol%, tubules were observed in all vesicles. Nearly all vesicles formed only one tubule, with < 1% forming a second, and the number of tubules was concentration independent. Below 5 mol% MPIase, tubule length was 5–30 μm; above 5 mol% MPIase, tubule lengths were likely > 30 μm, although they extended beyond the observation field. The mol% of MPIase shown in Fig. 2a represents the amount added outside the membrane, not the amount inserted into the membrane, which is less than the indicated percentage (Figure S1).

When used high-concentration KCl buffer (500 mM), tubule formation was not significantly reduced (79.0% ± 3.3%), indicating that electrostatic interactions play only a minor role in tubulation (Fig. 2b). Furthermore, adding 20 mol% mini-MPIase-3, a synthetic MPIase analog with only one trisaccharide unit (Figure S2)[9,10], instead of natural MPIase resulted in only 9.2% ± 6.0% of GUVs forming tubules (Fig. 2b). This substantial reduction indicates that interactions between MPIase's longer sugar chains are crucial for tubule formation.

MPIase localization on tubule-forming GUVs

To investigate MPIase localization on tubule-forming GUVs, we added 20 mol% MPIase to POPC GUVs labeled with 0.1 mol% TR-DHPE and stained the MPIase molecules with anti-MPIase antibodies (αMPIase) and fluorescein isothiocyanate (FITC)-conjugated secondary antibodies (Fig. 3a). The FITC fluorescence probe, indicating the location of MPIase, preferentially localized to the base of the tubule (Fig. 3a and b). The observed fluorescence width was approximately 0.8 μm. Occasionally, more than one fluorescence appeared in a cross-section; however, even when two or three were observed, tubules elongated from only one fluorescence. When 5 mol% MPIase was premixed with POPC lipids at the initial GUV preparation stage, MPIase aggregates were also detected, but external tubules did not form (Fig. 3c). In this case, MPIase resided in both the inner and outer layers of GUVs, suggesting that the asymmetric distribution of MPIase in the lipid bilayers' outer layer is essential for tubule formation.

To further investigate the contribution of the sugar chains of MPIase to tubule formation on the lipid bilayer, a mixture of 10 mol% MPIase and 10 mol% nitrobenzoxadiazole (NBD)-mini-MPIase-3 was added to POPC/0.1 mol% TR-DHPE GUVs (Fig. 3d). In NBD-mini-MPIase-3, the fluorescent NBD group is attached to mini-MPIase-3 (Figure S3a). The GUVs formed a protruding tubule (Fig. 3d, top), and NBD-mini-MPIase-3 was uniformly distributed throughout the membrane, including the tubule, with no aggregation (Fig. 3d, bottom). Upon adding 20 mol% NBD-mini-MPIase-3 to POPC/0.1 mol% TR-DHPE GUVs without MPIase, it was also uniformly distributed without exhibiting aggregates (Figure S3b). These results suggest that long sugar chains enable MPIase to aggregate and reside at the base of tubules, with interactions among sugar chains playing a crucial role in both MPIase aggregate and tubule formation.

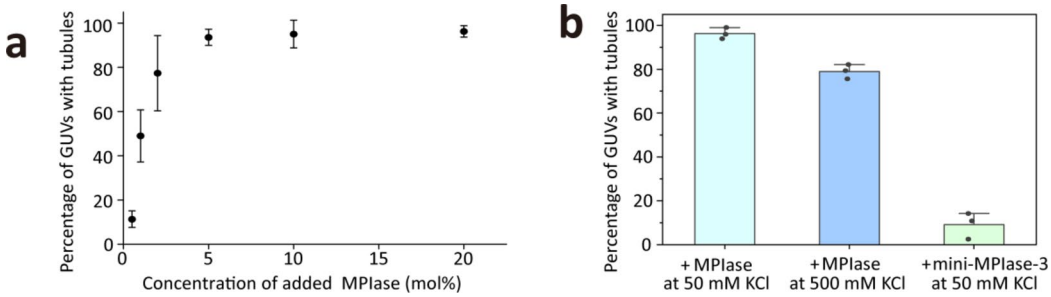

Fig. 2. (**a**) Percentage of GUVs forming tubules as a function of MPIase concentration. (**b**) Percentage of GUVs forming tubules after adding 20 mol% MPIase (left and middle) or mini-MPIase-3 (right) and incubating for 2 h at varying KCl concentrations. Error bars in (**a**) and (**b**) represent standard deviations from three independent experiments, with > 100 GUVs observed per condition.

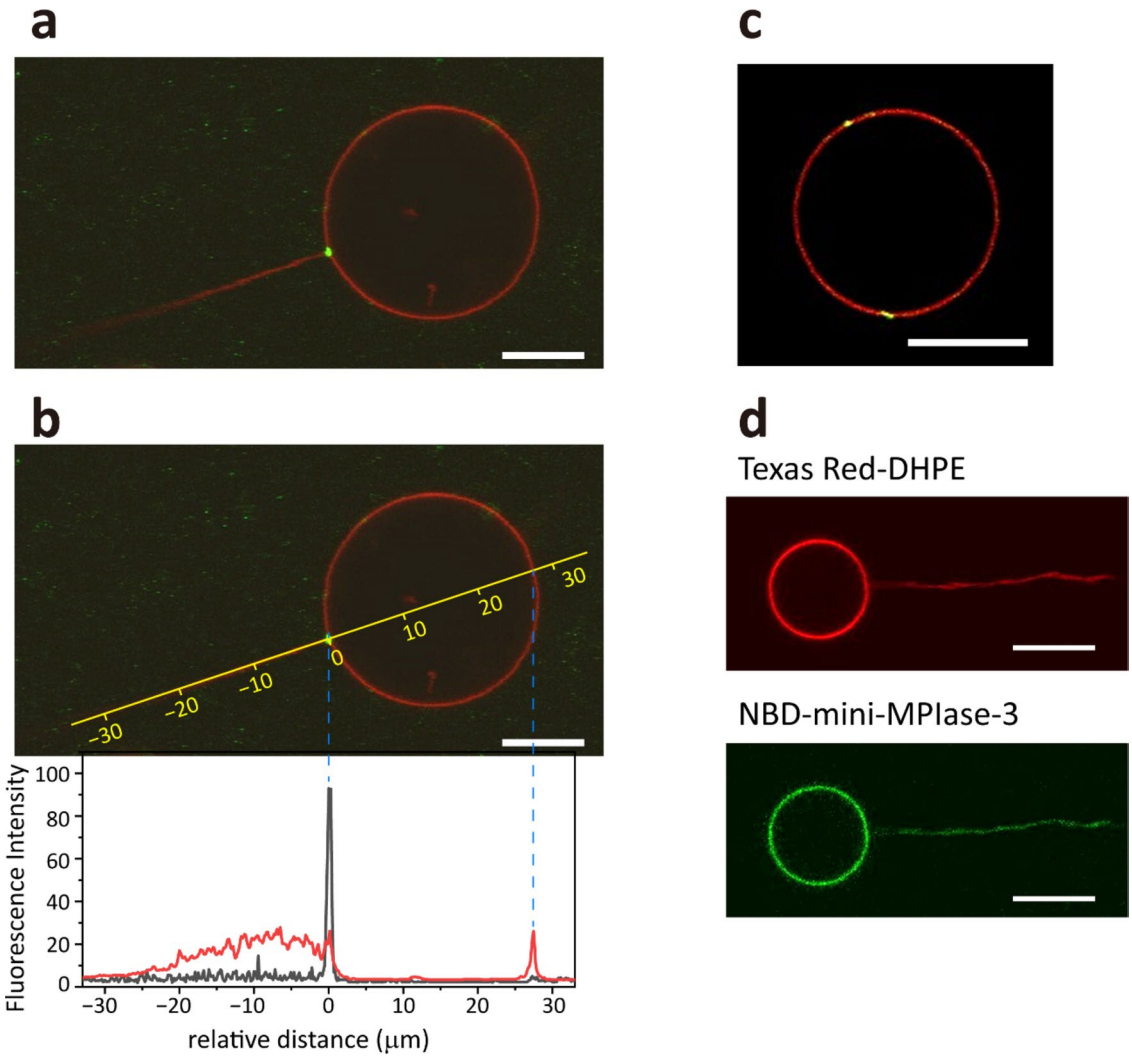

Fig. 3. (**a**) Merged confocal fluorescence image of a POPC GUV labeled with 0.1 mol% TR-DHPE preincubated with 20 mol% MPIase for 2 h prior to staining with anti-MPIase antibody (αMPIase) and FITC-conjugated secondary antibody (green). Fluorescence was observed exclusively at the base of the tubule. (**b**) Intensity distribution (bottom) of the Texas Red (red) and FITC (black) along the yellow line (top) across the tubule shown in (**a**). (**c**) Merged confocal fluorescence image of a POPC/0.1 mol% TR-DHPE/5 mol% MPIase GUV treated with αMPIase and FITC-conjugated secondary antibodies, where MPIase was mixed with POPC lipid at the start of GUV preparation. (**d**) Confocal fluorescence images of a POPC GUV/0.1 mol% TR-DHPE after adding a mixture of 10 mol% MPIase/10 mol% nitrobenzoxadiazole (NBD)-mini-MPIase-3. Scale bars in (**a**–**d**): 10 μm.

We also examined variations in tubule formation, performing an experiment (Fig. 3a) using GUVs composed of commercially available *E. coli* phospholipids (EPLs), which contain only phosphatidylethanolamine, phosphatidylglycerol, and cardiolipin. As shown in Fig. 3a, a single tubule formed on the EPL membrane, with MPIase residing at the base (Figure S4), implying that MPIase aggregation is not dependent on lipid type and likely occurs in *E. coli* cell membranes. Additionally, we examined another glycolipid, enterobacterial common antigen (ECA), found in the outer membranes of *E. coli*. ECA's structure closely resembles that of MPIase, but its sugar chain is linked to DAG via monophosphate rather than pyrophosphate (Figures S5a and b)[26–28]. We prepared an *E. coli* outer membrane extract mainly composed of ECA and added 20 mol% ECA (Figure S5c) to the POPC GUVs. This also resulted in tubulation on the GUVs, suggesting that pyrophosphate is not required for tubule formation or for aggregation at the base of the tubules.

Distribution of membrane aggregates on the supported planar lipid bilayer

To observe the distribution of MPIase on POPC membranes, we prepared a supported planar lipid bilayer (SPB) from POPC, added 20 mol% MPIase, and treated the SPB with αMPIase and FITC-conjugated secondary antibodies. The POPC planar membranes were confined in 20 × 20 μm compartments separated by a polymerized lipid bilayer[29]. MPIase aggregation was observed on the SPB (Fig. 4a, inset). Figure 4a shows the histogram of

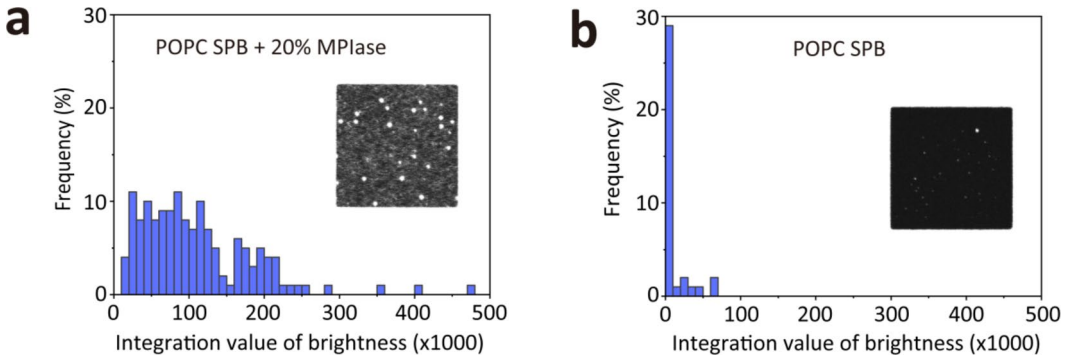

Fig. 4. Histogram of individual particles' fluorescence intensities observed on POPC SPBs treated with αMPIase and FITC-conjugated secondary antibodies. Samples were preincubated with MPIase for 2 h prior to adding the antibodies in (**a**), whereas MPIase was not preincubated in (**b**). The fluorescence images from six frames shown in Figure S6 were used to generate each histogram. The insets in both histograms show the representative images.

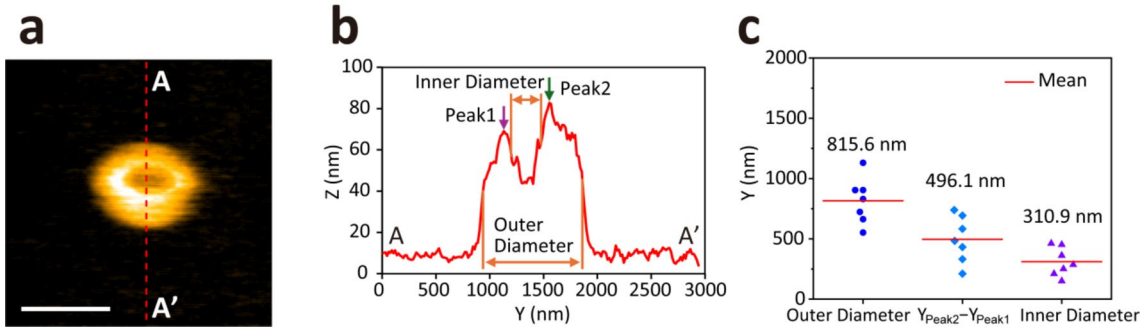

Fig. 5. (a) Representative image of a membrane bud induced by adding 1.5 mol% MPIase to the supported POPC lipid bilayer, as observed via high-speed atomic force microscopy (HS-AFM). A dimple is visible at the center of the structure. Scale bar: 1 µm. (**b**) Height profile of the structure's cross-section along the red dotted line A–A' in (**a**). (**c**) Diameters and peak-to-peak distance (Y_{peak2}–Y_{peak1}) of cross-sections from seven examined structures. The definitions of outer and inner diameters are provided in Figure S7. Red bars indicate mean values. Their values along the X-and Y-axes are shown in Table S1.

fluorescence intensities of the aggregates (Figure S6), indicating aggregate formations of different sizes. When the procedure was repeated without MPIase, no aggregation was observed (Fig. 4b). These findings suggest that multiple aggregates likely exist on the GUVs, but that only one MPIase aggregate forms a tubule on each vesicle.

Fine structures of membrane buds on the planar lipid bilayer

The fine structures of buds formed by MPIase aggregates on the lipid bilayer were observed using high-speed atomic force microscopy (HS-AFM; Fig. 5a). A supported POPC bilayer was formed on a flat mica surface, to which 1.5 mol% MPIase was added in the aqueous phase (Fig. 5a). Humped structures measuring 815.6 ± 189.9 nm in diameter were observed on the membrane (Fig. 5b and c). Each structure featured a central dimple measuring 310.9 ± 119.2 nm in diameter (Fig. 5a–c; Table S1). These structures were absent without MPIase, suggesting that MPIase aggregates are formed on them. The height of the structures above the lipid bilayer was around 60–70 nm, markedly taller than the glycan moiety of MPIase (< 20 nm). This height (Fig. 5b) likely represents the combined height of the glycan moiety and the protruding membrane. In contrast to tubule formation observed in GUVs (Figs. 1b and 3a), the membrane measured via HS-AFM showed a slight protrusion that did not elongate into tubules (Fig. 5). This difference may stem from the interaction between the mica plate and the lipid bilayer, which likely increases the membrane's resistance to movement. When we performed the same experiment with 0.1 mol% of MPIase, we observed comparable sized humped structures measuring 958.7 ± 205.5 nm in diameter (Figure S8, Table S2); however, the number of structures was significantly lower. These results suggest that the initial nucleation for the aggregates depends on MPIase concentration and is time-consuming, whereas the subsequent assembly of MPIase molecules around the nucleus proceeds independently of the concentrations, resulting in aggregates of a certain size.

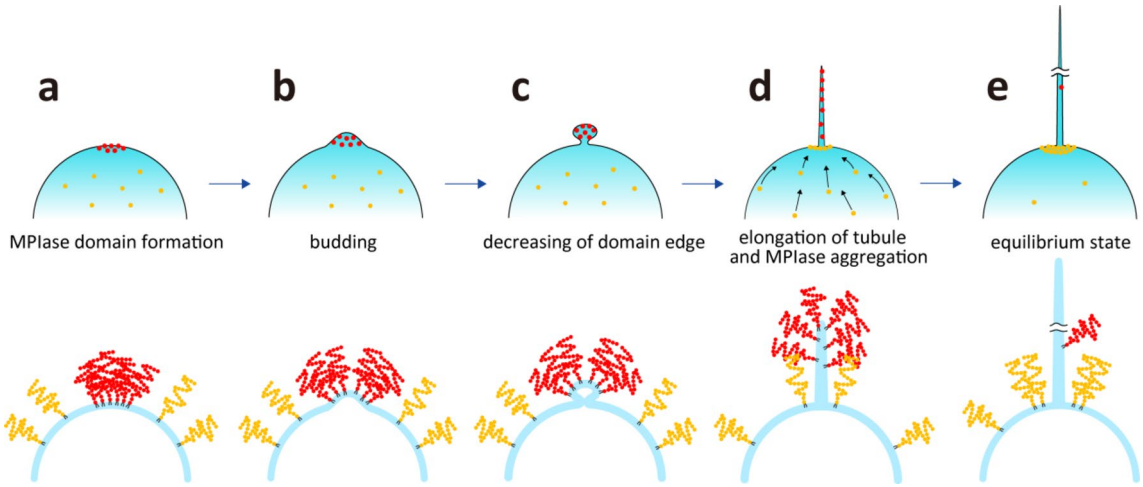

Fig. 6. Proposed mechanism of membrane tubule formation. (**a**) MPIase distributed asymmetrically outside the membrane forms aggregates on the membrane surface through sugar chain–sugar chain interactions. Red dots represent the MPIase responsible for membrane tubulation, whereas orange dots indicate other MPIase molecules. (**b**) One of the MPIase aggregate (red dots) induces spontaneous surface curvature by steric crowding, forming a membrane bud. (**c**) Line tension at the domain edge shortens its length. (**d**) Constricted membrane buds elongate into long tubules to minimize the elastic energy for a given area difference between the outer and inner membrane leaflets. Membrane lipids flow to elongate the tubule. Nontubule-forming MPIase (orange dots) is displaced toward the tubule tip together with the membrane lipids, but accumulates at the tubule base, forming aggregates as it does not favor negative curvature. The transition form (**c**) is hypothetical. (**e**) Final state where tubule elongation due to the area difference is complete. The omitted tubule section is indicated by a break line. Early MPIase aggregates diffuse along the tubule, whereas later aggregates are observed at the tubule base. Cross-sectional views are presented in the lower panel, with MPIase schematically depicted.

Discussion

MPIase is a glycolipid essential for membrane protein integration. In addition, in this study, we found MPIase-induced membrane tubulation and elucidated its mechanism using various microscopic techniques. The formation of microstructures during processes such as endocytosis, exocytosis, and cytokinesis is vital for cell physiology; thus, the mechanisms of membrane shape change have been studied extensively[30]. Most research has focused on tubulation driven by an increase in spontaneous curvature induced by membrane-bound proteins. These tubulation mechanisms can be categorized into two types. The first type is scaffolding proteins, including BAR domain proteins[19–21]and septin cytoskeletal proteins[22], which form the membrane tubules while binding to the membrane. The bulky disordered regions of BAR domain proteins work synergistically with BAR domains to facilitate membrane fission[23]. The other type is membrane-bound proteins, which increase spontaneous curvature through crowding of their moieties, causing the membrane to protrude. For instance, epsins bind to the membrane via phosphatidylinositol, curving the membrane due to simple protein proximity[24]. Other membrane-bound proteins with intrinsically disordered regions can undergo liquid–liquid phase separation near the membrane, resulting in inward tubulation[31].

Although proteins are the primary drivers of many membrane deformation processes, the glycolipid ganglioside GM1 has been shown to induce tubulation on GUVs in vitro. GM1, a sialic acid-containing glycosphingolipid abundant in vertebrate neuronal cell membranes, plays key roles in various physiological processes, including neurotransmission and neuronal differentiation[32]. Composed of ceramide linked to a branched sugar chain with five sugars, GM1 has been reported to induce either inward or outward tubules, depending on which bilayer leaflet exhibits greater GM1 distribution[16].

LPS, another glycolipid, induces a different type of membrane deformation compared to tubulation. LPS is a major component of the outer layer of gram-negative bacteria and a potent inducer of the innate immune response[33]. It binds to the membrane via six acyl chains attached to two glucosamines, along with a long sugar chain lacking acetyl groups[34], unlike MPIase. Alam et al. reported that prolate DOPC GUVs transition from a pear shape to two asymmetric spheres connected by a narrow neck following LPS addition outside GUVs[18]. The authors explained the shape change using the area-difference elasticity model[35,36], where the elastic energy of a GUV is expressed as the sum of membrane bending energy and the energy from relative monolayer stretching. Adams et al. found that LPS addition to fluid-phase supported lipid bilayer assemblies resulted in long, flexible, strand-like lipid structures formed from merging surface-associated lipid vesicles. However, this process differs from the tubules observed in the present study.

Based on our findings, we propose a mechanism for tubule formation induced by MPIase (Fig. 6). Curvature-inducing proteins, when locally distributed on one side of a membrane, can theoretically induce tubules to sprout from lipid vesicles[37,38]. Similarly, MPIase aggregates likely form tubules on the membrane. In our study, MPIase was added only to the exterior of the membrane. As indicated by the distribution of NBD-mini-MPIase-3,

we infer that MPIase is uniformly incorporated throughout the GUV upon addition. However, some MPIase subsequently aggregates (Fig. 6a). If the MPIase antibodies detect only the aggregates, we cannot observe MPIase which does not belong to the aggregates. We suggest that these MPIase aggregates (red dots in Fig. 6) generate spontaneous curvature through steric crowding[38] and form membrane buds (Fig. 6b).

When membranes laterally separate into domains with distinct compositions, vesicle geometry can be theoretically derived by minimizing energy from bending resistance and line tension[37,39]. We previously demonstrated that adding MPIase disorders lipid acyl chains and loosens membrane surface packing[12,13]. Consequently, lipids in membrane buds with dense MPIase exhibit different mobility and packing compared to those outside the bud, creating line tension at the domain edge that reduces its length (Fig. 6c). Subsequently, the constricted membrane buds elongate into long tubules to alleviate instability caused by area differences between the outer and inner leaflets[35,36] (Fig. 6d). Protruding a longer and narrower tubule from a limited GUV surface area is more effective for minimizing the elastic energy for a given internal and external area difference than a shorter and wider tubule. We observed that tubule length increased with higher MPIase concentrations, indicating that the destabilizing effect from area differences becomes more pronounced with higher MPIase levels. Given that only one tubule forms from almost every GUV, once tubule formation begins, membrane lipids likely flow to drive tubule elongation. MPIase on the GUV that does not form a membrane bud (orange dots in Fig. 6) migrates toward the tubule's tip along with the membrane lipids. However, although lipids can move into the tubule, MPIase accumulates at the tubule's base due to MPIase's large headgroup, which hinders passage through the area with negative curvature at the tubule's base (Fig. 6d). The detained MPIase forms aggregates through sugar chain–sugar chain interactions. Conversely, the pyrophosphate moiety of MPIase is charge-repulsive, leaving the area near the membrane surface spatially open. Consequently, membrane lipids moving toward the tubule tip can navigate among the acyl chains of MPIase (Fig. 6d)[17]. Thus, MPIase at the base of the tubule serves as a gate for membrane lipids, whereas MPIase on the tubule maintains positive curvature. Once tubule elongation is complete, MPIase on the tubule continues to diffuse, while the aggregates formed later are observed at the base (Fig. 6e). Although MPIase is present on both the tubule and the GUV itself, its concentration is too low for detection; only aggregated MPIase at the base of the tubule is visible under a fluorescence microscope (Fig. 3a, b).

As shown in HS-AFM images, the average outer diameter of membrane buds (815.6 ± 189.9 nm; Table S1) is greater than that of the tubules (68.0 ± 27.7 nm), as observed in negative-stain EM images (Fig. 1c–e). The former diameter corresponds to the membrane buds illustrated in Fig. 6b, whereas the latter corresponds to the elongated tubules shown in Fig. 6d. Based on the HS-AFM images (Fig. 5 and S8), we hypothesize that the redistribution of MPIase during membrane budding occurs as follows: When MPIase aggregates on membranes, steric crowding induces positive curvature, leading to the formation of a membrane bud. Subsequently, MPIase with a bulky headgroup tends to localize along the lateral sides of the bud, where higher positive curvature is present relative to the upper side. In contrast, the density of MPIase in the central part of the upper side is relatively lower. At the periphery of the upper side, MPIase molecules present in high density and induce positive curvature. In this way, the redistribution of MPIase, which causes the variation in glycan density and the curvature, likely contributes to the ring-like structure observed via HS-AFM (Fig. 5a and b).

Regarding MPIase aggregation, sugar chains appear to play a key role. MPIase positions its sugar chains outside the membrane, whereas its lipid segment is embedded in the membrane. The interaction between these extended sugar chains likely drives aggregation, as supported by the observation that mini-MPIase-3 did not aggregate on the membrane (Fig. 3b). Each MPIase amino sugar carries an *N*-acetyl group, with approximately one-third of GlcNAc also featuring an *O*-acetyl group. Hydrophobic interactions between these acetyl groups likely contribute to MPIase aggregation. Additionally, tubules were still observed at high salt concentrations (500 mM KCl), indicating that electrostatic interactions do not make a major contribution to MPIase aggregation.

For LPS-induced tubulation, pear-shaped deformation has previously been explained by the area difference between the inner and outer membrane layers, similar to the elongation stage in MPIase-induced tubulation. However, LPS requires cross-linking with divalent cations to form aggregates, whereas MPIase aggregates independently of such ions. The larger head-to-tail width ratio of MPIase compared to LPS, given its fewer acyl chains, may enhance MPIase aggregation on the membrane. These differences likely explain why MPIase initially forms membrane buds before elongating into tubules, whereas LPS induces pear-shaped deformation without budding. Although both MPIase and LPS are glycolipids with long sugar chains and components of the *E. coli* membrane, they deform membranes through different mechanisms.

Comparing MPIase-driven tubulation with protein-driven processes, the mechanisms differ fundamentally. Membrane-bound proteins require specific membrane lipids for binding, whereas MPIase's lipid component anchors its head moiety to the membrane. Despite these differences, given their similar structures after membrane binding, both MPIase and membrane-bound proteins induce spontaneous curvature through steric crowding, resulting in tubule formation. However, MPIase forms more compact aggregates on the membrane compared with epsin, a representative membrane-bound protein[24]. This may explain MPIase's distinct distribution after tubule formation compared to membrane-bound proteins.

In the context of tubule formation by proteins, Takiguchi et al. categorized two distinct types of tubulation, depending on the number of tubules formed on a membrane[40]: (i) a limited number of tubules, usually one or a few, arising from a specific region on the membrane surface; or (ii) the simultaneous development of multiple tubules, with dozens forming across the GUV surface. These tubulation processes are characterized by the elongation rate of the tubules[40]. In case (i), the elongation rate is significantly faster than the initiation of tubule formation. In contrast, in case (ii), many tubules form simultaneously, and the elongation of each tubule proceeds more slowly than in case (i). Our study revealed that MPIase induces only one tubule per GUV in almost all observations, corresponding to case (i). The results obtained from fluorescence microscopy (Figs. 1b and 3a) and AFM measurement (Fig. 5and S8) also suggest that the formation of membrane buds is a time-

consuming process because it occurs only after aggregates of a certain size have formed. However, once a single tubule begins to elongate, it elongates rapidly, and lipids on the GUV are mobilized toward the tubule tip to support the tubule's growth. As a result, it becomes difficult for additional tubules to elongate from other MPIase aggregates. Takiguchi et al. also highlighted that the tubules in case (ii) are more rigid than those in case (i), based on measurements of the tubule bending modulus, suggesting a higher density of proteins associated with the tubules in case (ii) than in case (i)[40]. In their study of force measurements using two polystyrene beads encapsulating GUVs without any other additives such as proteins, it was reported that the force required to develop a new tubule on a pure liposome is much greater than that required to elongate a tubule[41]. Thus, tubule elongation inherently takes less time than membrane bud formation, but higher density of tubule-inducing molecules on the tubules reduces the rate of the elongation. In our case, the density of MPIase in the tubules was low as shown in Fig. 3a. This is one of the reasons why we hypothesize that MPIase-induced tubulation corresponds to case (i).

The tubule formation induced by MPIase, as observed in our experiments, may have functional implications related to the roles of glycolipids in *E. coli*. MPIase's primary function is to facilitate the integration of proteins into membranes. We previously revealed the mechanism for Sec-independent membrane insertion of a small hydrophobic protein as follows[9–13]: (i) MPIase prevents nascent proteins from aggregating by capturing them with its sugar chains and delivers them into the membrane surface through the interaction with pyrophosphate; (ii) MPIase alters the physicochemical properties of membranes, such as loosening of the membrane surface packing and increasing the mobility in the membrane core, which facilitates the insertion. In addition, the ability of MPIase to induce tubule formation may further enhance its role in membrane integration. It is known that generating positive curvature on membrane surfaces creates crevices that facilitate protein integration. For example, the 18-residue *N*-terminal peptide of epsin promotes membrane tubule formation by increasing membrane curvature and inserts into the membrane[42,43]. As the tubule regions adopt a lipid bilayer structure but have a much higher curvature than other region of liposomes, which may allow easier insertion of proteins through this tubular region.

Beyond aiding membrane protein integration, the tubule formation resulting from MPIase aggregation may serve an additional role in vesicle release. After BAR domain protein-induced tubule formation, membrane tubules can be released as vesicles through the scission by scaffolding protein such as Dynamin[44]. In addition, Nishimura et al. reported that vesiculation of membrane tubules induced by one of the BAR domain proteins, MIM, occurred upon the application of external forces at levels typically observed in vivo[45]. Given that *E. coli* does not possess BAR domain proteins, the regulation of membrane dynamics, including vesicle release, must be mediated by other molecules or external forces. In general, *E. coli* releases numerous membrane vesicles into the extracellular environment[46,47], and the tubule-forming ability of ECA (Figure S5c) may be related to this process. Although MPIase is typically added from the cytoplasm side, its localization in the membrane or increased biosynthesis could lead to higher local concentrations, potentially inducing membrane deformation. In such cases, MPIase may also play a role in releasing membrane vesicles into the cytoplasm.

In conclusion, we demonstrated that MPIase forms aggregates on membranes, which then trigger the formation of tubular protrusions, specifically when MPIase is asymmetrically distributed on the outer layer of the lipid bilayer. Notably, aggregates were observed at the base of tubules after their formation. Electrostatic interactions are not crucial for tubulation, suggesting that the acetyl groups on sugar components of MPIase play a major role in this process. Based on these findings, we propose a novel mechanism for MPIase-induced membrane tubulation. This glycolipid-mediated mechanism highlights previously unrecognized roles of glycolipids in membrane dynamics. Further analysis of MPIase assembly, alongside other cytosolic molecules on the membrane, will deepen our understanding of the diverse functions of glycolipids in complex physiological environments.

Materials and methods

Materials

EPL and POPC were purchased from Avanti Polar Lipids (Alabaster, AL, USA). TR-DHPE was obtained from Molecular Probes (Eugene, OR). All lipids were used without further purification. MPIase was purified from *E. coli* strain MC4100 following previously described methods[2]. The anti-MPIase antibody was raised in rabbits using purified MPIase crosslinked to keyhole limpet hemocyanin. MPIase analogs, mini-MPIase-3 and NBD-mini-MPIase-3, were synthesized as previously described[10]. FITC-conjugated goat anti-rabbit IgG antibody was purchased from Proteintech (Chicago, IL). The anti-ECA antibody and Alexa Fluor 488–conjugated goat anti-mouse IgG antibody were purchased from Invitrogen (Carlsbad, CA). Additionally, 6-carboxyfluorescein was purchased from Novabiochem (Darmstadt, Germany).

Preparation of GUVs

Mixtures of POPC and 0.1 mol% TR-DHPE were dissolved in chloroform/methanol (9/1, v/v) solution. The solvent was evaporated under a stream of nitrogen gas, and the lipids were dried under a vacuum overnight to ensure complete solvent removal. The dried lipid film was gently hydrated with a 150-mOsm sucrose solution at 40 °C to achieve a final concentration of 1 mM. GUVs formed via lipid swelling during overnight incubation.

Observation of tubule formation upon external addition of MPIase

To monitor tubule formation, 1 mM GUV suspensions were diluted 100-fold in buffer A [25 mM Tris-HCl and 50 mM KCl (pH 7.6)] and placed in a round sample chamber. Designated amounts of MPIase or mini-MPIase-3 were added externally to the chamber. To prevent vesicle adhesion, cover glasses were coated with an amorphous perfluorinated polymer, CYTOP CTL-107MK (Asahi Glass Co., Ltd., Tokyo, Japan). The osmolarity of all buffers was matched to that of the GUV solution. To quantify the percentage of GUVs with lipid tubules, more than

80 GUVs were counted, and the percentage containing tubules was calculated. Data were collected from three independent GUV batches. Only cases where tubule presence or absence was unambiguous were counted.

Distribution of MPIase on patterned polymeric supported membranes

Patterned polymeric bilayers were prepared as described previously[48]. Briefly, monomeric DiynePC bilayers were deposited onto cleaned cover glass substrates and polymerized using ultraviolet (UV) irradiation. A pattern of square compartments (20 × 20 μm) separated by 5-μm borders was created during polymerization by illuminating the sample through a photomask placed directly on the DiynePC bilayer. After UV irradiation, the compartments were formed by immersing the sample in a 0.1 M SDS solution. A sample chamber was created by attaching a silicone rubber ring (12-mm diameter) to the glass substrate. After adding phosphate-buffered saline to the chamber, 1 mM POPC small unilamellar vesicle suspensions were applied to the substrate, incubated for 30 min, and thoroughly rinsed with Milli-Q water. To observe MPIase distribution on the POPC membranes, the buffer was replaced with buffer A, and 20 mol% MPIase was added. After 2 h of incubation, the SPB was treated with αMPIase and FITC-conjugated secondary antibodies, incubating each antibody for 1 h.

Fluorescence microscopy

GUVs and SPBs were imaged using a confocal laser-scanning microscope (FLUOVIEW FV3000; Olympus, Tokyo, Japan) equipped with an oil immersion objective lens (LUCPLFLN 100×, NA 1.45) at room temperature. For excitation, lasers with wavelengths of 561 and 488 nm were used, and the fluorescence signals were collected in the ranges 570–620 and 500–540 nm, respectively. Images were acquired using FV31S-SW software, and the contrast and brightness of the images were adjusted using ImageJ software. To count GUVs with tubules, images were captured using a microscope-attached digital camera (WRAYCAM-VEX830; Wraymer, Osaka, Japan) and analyzed using MicroStudio software (Wraymer).

Electron microscopy

Specimens for EM were prepared via negative staining, as described previously[49]. A 2-mL sample, containing 20 mol% MPIase added to the POPC GUV, was applied to a copper grid mesh (Cu 200, JEOL, 780111621) that was covered with a thin carbon film and pretreated with a hydrophilic glow discharge for 1 min. After 1 min of sample deposition, excess solution was blotted from the grid's backside, and the residual salt was washed away twice with 2 mL of Milli-Q water. Subsequently, 2 mL of 2% aqueous phosphotungstic acid solution was placed on the grid for 1 min, and excess solution was removed with filter paper. Samples were dried gently in a desiccator containing silica gel, and images were acquired using a JEM-2200FS (JEOL Ltd., Tokyo, Japan) equipped with a Rio 9 CCD camera (Gatan, USA) at an acceleration voltage of 200 kV. Tubule diameters were analyzed using ImageJ software.

High-speed atomic force microscopy

AFM imaging was performed using a laboratory-built HS-AFM apparatus, as reported previously[50,51]. HS-AFM imaging was performed in tapping mode, with cantilever deflection detected using an optical beam deflection detector. The laser beam was focused onto a small cantilever [$0.1 \le k \le 0.2$ N/m and $600 \le f \le 1200$ kHz in solution (Olympus, Tokyo, Japan)], where k and f are the spring constant and resonant frequency, respectively. AFM styli were grown on each cantilever using electron-beam deposition and sharpened via plasma etching. A 1.5-mm-diameter mica disk was glued to a quartz sample stage. MPIase aggregates were formed on the mica surface following a procedure similar to the fluorescence microscopy experiment using a patterned membrane. A 1.5-μL droplet of 1 mM POPC was deposited onto freshly cleaved mica and incubated for over 1 h to form an SPB. The mica surface was then rinsed with buffer A to remove excess small unilamellar vesicles. A 1.5-μL droplet of MPIase with a concentration of ~ 0.7 ng/μL in buffer A was placed on the mica surface. This MPIase concentration corresponds to 1.5 mol% of POPC on the mica. After 1 h of incubation at 25 °C, the mica surface was rinsed with buffer A, and HS-AFM measurements were performed at room temperature under buffer A. To perform HS-AFM observations with 0.1 mol% MPIase, a 1.5-μL droplet of MPIase solution with a concentration of ~ 0.047 ng/μL was placed onto a mica surface that had been prepared by depositing 1.5-μL droplet of 2 mM POPC.

Purification of enterobacterial common antigen

ECA was prepared as previously described[2,52]. Briefly, outer membranes purified from *E. coli* strain MC4100 were extracted with 6% sodium cholate. The extract was precipitated with 80% acetone, and the precipitate was washed successively with acetone and diethyl ether. The dried precipitate was further treated with a phenol/chloroform/hexane mixture (2/5/8) following Galanos et al.[53]. After chloroform and hexane were removed under a nitrogen stream, LPS was precipitated by adding a few drops of water to the phenol phase. The supernatant was then extensively dialyzed, and the sample was isolated via partition chromatography on a Sephadex LH-20 column. The column was equilibrated using the aqueous phase of solvent A (1-butanol/tetrahydrofuran/ethanol/water, 8/7/1/20) and developed using the organic phase of solvent A. Fractions showing only one brown spot upon thin layer chromatography analysis were collected. The dried sample was dissolved in water/ethanol (1/1), and the dried supernatant was redissolved in chloroform/methanol/water (3/2/1). The water phase was collected, and the purified ECA preparation was analyzed using western blotting (Figure S5b).

Data availability

The datasets generated during the study are available from the corresponding author upon reasonable request.

Received: 22 October 2024; Accepted: 7 March 2025
Published online: 20 March 2025

References

1. Nishiyama, K. et al. A derivative of lipid A is involved in signal recognition particle/SecYEG-dependent and -independent membrane integrations. *J. Biol. Chem.* **281**, 35667–35676 (2006).
2. Nishiyama, K. et al. A novel complete reconstitution system for membrane integration of the simplest membrane protein. *Biochem. Biophys. Res. Commun.* **394**, 733–736 (2010).
3. Nishiyama, K. et al. MPIase is a glycolipozyme essential for membrane protein integration. *Nat. Commun.* **3**, 1260 (2012).
4. du Plessis, D. J., Nouwen, N. & Driessen, A. J. The sec translocase. *Biochim. Biophys. Acta*. **1808**, 851–865 (2011).
5. Luirink, J., von Heijne, G., Houben, E. & de Gier J. W. Biogenesis of inner membrane proteins in Escherichia coli. *Annu. Rev. Microbiol.* 59, 329–355 (2005).
6. Wolfe, P. B., Rice, M. & Wickner, W. Effects of two sec genes on protein assembly into the plasma membrane of Escherichia coli. *J. Biol. Chem.* **260**, 1836–1841 (1985).
7. Geller, B. L. & Wickner, W. M13 procoat inserts into liposomes in the absence of other membrane proteins. *J. Biol. Chem.* **260**, 13281–13285 (1985).
8. Kiefer, D., Hu, X., Dalbey, R. & Kuhn, A. Negatively charged amino acid residues play an active role in orienting the Sec-independent Pf3 coat protein in the Escherichia coli inner membrane. *EMBO J.* **16**, 2197–2204 (1997).
9. Fujikawa, K. et al. Structural requirements of a glycolipid MPIase for membrane protein integration. *Chem. Eur. J.* **29**, e202300437 (2023).
10. Fujikawa, K. et al. Syntheses and activities of the functional structures of a glycolipid essential for membrane protein integration. *ACS Chem. Biol.* **13**, 2719–2727 (2018).
11. Mori, S. et al. Intermolecular interactions between a membrane protein and a glycolipid essential for membrane protein integration. *ACS Chem. Biol.* **17**, 609–618 (2022).
12. Nomura, K. et al. Role of a bacterial glycolipid in Sec-independent membrane protein insertion. *Sci. Rep.* **12**, 12231 (2022).
13. Nomura, K. et al. Alteration of membrane physicochemical properties by two factors for membrane protein integration. *Biophys. J.* **117**, 99–110 (2019).
14. Kawashima, Y., Miyazaki, E., Müller, M., Tokuda, H. & Nishiyama, K. i. Diacylglycerol specifically blocks spontaneous integration of membrane proteins and allows detection of a Factor-assisted integration. *J. Biol. Chem.* **283**, 24489–24496 (2008).
15. Johannes, L., Wunder, C. & Shafaq-Zadah, M. Glycolipids and lectins in endocytic uptake processes. *J. Mol. Biol.* (2016).
16. Dasgupta, R., Miettinen, M. S., Fricke, N., Lipowsky, R. & Dimova, R. The glycolipid GM1 reshapes asymmetric biomembranes and giant vesicles by curvature generation. *Proc. Natl. Acad. Sci. U S A*. **115**, 5756–5761 (2018).
17. Adams, P. G., Lamoureux, L., Swingle, K. L., Mukundan, H. & Montaño, G. A. Lipopolysaccharide-induced dynamic lipid membrane reorganization: tubules, perforations, and stacks. *Biophys. J.* **106**, 2395–2407 (2014).
18. Alam, J. M. & Yamazaki, M. Spontaneous insertion of lipopolysaccharide into lipid membranes from aqueous solution. *Chem. Phys. Lipids*. **164**, 166–174 (2011).
19. Farsad, K. et al. Generation of high curvature membranes mediated by direct endophilin bilayer interactions. *J. Cell. Biol.* **155**, 193–200 (2001).
20. Itoh, T. et al. Dynamin and the actin cytoskeleton cooperatively regulate plasma membrane invagination by BAR and F-BAR proteins. *Dev. Cell.* **9**, 791–804 (2005).
21. Peter, B. J. et al. BAR domains as sensors of membrane curvature: the amphiphysin BAR structure. *Science* **303**, 495–499 (2004).
22. Tanaka-Takiguchi, Y., Kinoshita, M. & Takiguchi, K. Septin-mediated uniform bracing of phospholipid membranes. *Curr. Biol.* **19**, 140–145 (2009).
23. Snead, W. T. et al. BAR scaffolds drive membrane fission by crowding disordered domains. *J. Cell. Biol.* **218**, 664–682 (2019).
24. Stachowiak, J. C. et al. Membrane bending by protein-protein crowding. *Nat. Cell. Biol.* **14**, 944–949 (2012).
25. Yuan, C. & Johnston, L. J. Distribution of ganglioside GM1 in L-alpha-dipalmitoylphosphatidylcholine/cholesterol monolayers: a model for lipid rafts. *Biophys. J.* **79**, 2768–2781 (2000).
26. Basu, S., Kuhn, H. M., Neszmelyi, A., Himmelspach, K. & Mayer, H. Chemical characterization of enterobacterial common antigen isolated from Plesiomonas shigelloides ATCC 14029. *Eur. J. Biochem.* **162**, 75–81 (1987).
27. Bruix, M., Jiménez-Barbero, J. & Cronet, P. Determination by NMR spectroscopy of the structure and conformational features of the enterobacterial common antigen isolated from Escherichia coli. *Carbohydr. Res.* **273**, 157–170 (1995).
28. Kuhn, H. M., Meier-Dieter, U. & Mayer, H. ECA, the enterobacterial common antigen. *FEMS Microbiol. Rev.* **4**, 195–222 (1988).
29. Okazaki, T. et al. Polymerized lipid bilayers on a solid substrate: morphologies and obstruction of lateral diffusion. *Langmuir* **25**, 345–351 (2009).
30. Stachowiak, J. C., Brodsky, F. M. & Miller, E. A. A cost-benefit analysis of the physical mechanisms of membrane curvature. *Nat. Cell. Biol.* **15**, 1019–1027 (2013).
31. Yuan, F. et al. Membrane bending by protein phase separation. *Proc. Natl. Acad. Sci. U. S. A.* 118 (2021).
32. Ledeen, R. W. & Wu, G. The multi-tasked life of GM1 ganglioside, a true factotum of nature. *Trends Biochem. Sci.* **40**, 407–418 (2015).
33. Brade, H., Opal, S. M., Vogel, S. N. & Morrison, D. C. *Endotoxin in Health and Disease* (Marcel Dekker, Inc., 1999).
34. Rietschel, E. T., Brade, L., Lindner, B. & Zahringer, U. Biochemistry of lipopolysaccharides in *Bacterial endotoxic lipopolysaccharides* (eds Morison, D. C. & Ryan, J.) L.) 3–41 (CRC press, Inc., (1992).
35. Heinrich, V. V., Svetina, S. & Zeks, B. Nonaxisymmetric vesicle shapes in a generalized bilayer-couple model and the transition between oblate and prolate axisymmetric shapes. *Phys. Rev. E Stat. Phys. Plasmas Fluids Relat. Interdiscip Top.* **48**, 3112–3123 (1993).
36. Miao, L., Seifert, U., Wortis, M. & Döbereiner, H. G. Budding transitions of fluid-bilayer vesicles: the effect of area-difference elasticity. *Phys. Rev. E Stat. Phys. Plasmas Fluids Relat. Interdiscip Top.* **49**, 5389–5407 (1994).
37. Alimohamadi, H., Vasan, R., Hassinger, J. E., Stachowiak, J. C. & Rangamani, P. The role of traction in membrane curvature generation. *Mol. Biol. Cell.* **29**, 2024–2035 (2018).
38. Rangamani, P., Mandadap, K. K. & Oster, G. Protein-induced membrane curvature alters local membrane tension. *Biophys. J.* **107**, 751–762 (2014).
39. Lipowsky, R. Budding of membranes induced by intramembrane domains. *J. Phys. II.* **2**, 1825–1840 (1992).
40. Tanaka-Takiguchi, Y. et al. Physicochemical analysis from real-time imaging of liposome tubulation reveals the characteristics of individual F-BAR domain proteins. *Langmuir* **29**, 328–336 (2013).
41. Inaba, T. et al. Formation and maintenance of tubular membrane projections require mechanical force, but their elongation and shortening do not require additional force. *J. Mol. Biol.* **348**, 325–333 (2005).
42. Murayama, T. et al. Loosening of lipid packing promotes oligoarginine entry into cells. *Angew Chem. Int. Ed. Engl.* **56**, 7644–7647 (2017).
43. Pujals, S. et al. Curvature engineering: positive membrane curvature induced by Epsin N-terminal peptide boosts internalization of octaarginine. *ACS Chem. Biol.* **8**, 1894–1899 (2013).
44. Ferguson, S. M. & De Camilli, P. Dynamin, a membrane remodelling GTPas. *Nat. Rev. Mol. Cell. Biol.* **13**, 75–88 (2012).

45. Nishimura, T. et al. Filopodium-derived vesicles produced by MIM enhance the migration of recipient cells. *Dev. Cell.* **56**, 842–859e848 (2021).
46. Schwechheimer, C. & Kuehn, M. J. Outer-membrane vesicles from Gram-negative bacteria: biogenesis and functions. *Nat. Rev. Microbiol.* **13**, 605–619 (2015).
47. Schwechheimer, C., Sullivan, C. J. & Kuehn, M. J. Envelope control of outer membrane vesicle production in Gram-negative bacteria. *Biochemistry* **52**, 3031–3040 (2013).
48. Morigaki, K. et al. Surface functionalization of a polymeric lipid bilayer for coupling a model biological membrane with molecules, cells, and microstructures. *Langmuir* **29**, 2722–2730 (2013).
49. Hao, J., Ishihara, M., Rapenne, G. & Yasuhara, K. Lipid nanodiscs spontaneously formed by an amphiphilic polymethacrylate derivative as an efficient nanocarrier for molecular delivery to intact cells. *RSC Adv.* **14**, 6127–6134 (2024).
50. Tsuji, A., Yamashita, H., Hisatomi, O. & Abe, M. Dimerization processes for light-regulated transcription factor photozipper visualized by high-speed atomic force microscopy. *Sci. Rep.* **12**, 12903 (2022).
51. Yamashita, H. et al. Single-molecule imaging on living bacterial cell surface by high-speed AFM. *J. Mol. Biol.* **422**, 300–309 (2012).
52. Männel, D. & Mayer, H. Isolation and chemical characterization of the enterobacterial common antigen. *Eur. J. Biochem.* **86**, 361–370 (1978).
53. Galanos, C., Lüderitz, O. & Westphal, O. A new method for the extraction of R lipopolysaccharides. *Eur. J. Biochem.* **9**, 245–249 (1969).

Acknowledgements

This study was supported by JSPS KAKENHI (grant nos.:JP18K06143 and JP22K05323 for KA.N.; JP24KJ1579 for A.T.; JP22K18945, JP23H01818, and JP23H03073 for H.Y.; JP20K05738 and JP23K04955 for K.F.; JP24K17794 for S.M.; JP22H02567 and JP24H01107 for K-i.N.; JP19H02843 and JP22H02213 for K.S.) and by CiDER from Osaka University and Frontier Research Grant from the Japan Institute of Metals for H.Y. We thank S. Fujita and M. Fujihara for supporting the electron microscopy measurement.

Author contributions

KA.N. and K.S. designed the study. KA.N. and TO.O. performed the fluorescence microscopy experiments. A.T., H.Y., and M.A. performed the HS-AFM measurements. K.Y. performed the electron microscopy measurements. S.M. performed the NMR measurements. K.F., TS.O., K.S. and K-i.N. prepared MPIase and its analogues. KA.N., S.M., H.T., and K-i.N. prepared ECA. K.M. prepared patterned polymeric bilayers. KA.N. and K.S. wrote and edited the manuscript with contributions from all authors.

Competing interests

The authors declare no competing interests.

Supplementary Information

The online version contains supplementary material available at http://doi.org/…….
Correspondence and requests for materials should be addressed to K.NR. and K.S.

Additional information

Supplementary Information The online version contains supplementary material available at https://doi.org/10.1038/s41598-025-93563-8.

Correspondence and requests for materials should be addressed to K.N. or K.S.